



Bimodal distribution of the magnetic dipole moment in nanoparticles with a monomodal distribution of the physical size



Jos van Rijssel, Bonny W.M. Kuipers, Ben H. Ern  *

Van 't Hoff Laboratory for Physical and Colloid Chemistry, Debye Institute for Nanomaterials Science, Utrecht University, Padualaan 8, 3584 CH Utrecht, The Netherlands

ARTICLE INFO

Article history:

Received 30 June 2014

Received in revised form

22 September 2014

Accepted 29 September 2014

Available online 1 October 2014

Keywords:

Magnetic nanoparticles

Magnetic dipole moments

Magnetic domains

Magnetic polydispersity

Multimodal distributions

Magnetization curves

ABSTRACT

High-frequency applications of magnetic nanoparticles, such as therapeutic hyperthermia and magnetic particle imaging, are sensitive to nanoparticle size and dipole moment. Usually, it is assumed that magnetic nanoparticles with a log-normal distribution of the physical size also have a log-normal distribution of the magnetic dipole moment. Here, we test this assumption for different types of superparamagnetic iron oxide nanoparticles in the 5–20 nm range, by multimodal fitting of magnetization curves using the MINORIM inversion method. The particles are studied while in dilute colloidal dispersion in a liquid, thereby preventing hysteresis and diminishing the effects of magnetic anisotropy on the interpretation of the magnetization curves. For two different types of well crystallized particles, the magnetic distribution is indeed log-normal, as expected from the physical size distribution. However, two other types of particles, with twinning defects or inhomogeneous oxide phases, are found to have a bimodal magnetic distribution. Our qualitative explanation is that relatively low fields are sufficient to begin aligning the particles in the liquid on the basis of their net dipole moment, whereas higher fields are required to align the smaller domains or less magnetic phases inside the particles.

   2014 Elsevier B.V. All rights reserved.

1. Introduction

High-frequency biomedical applications of magnetic nanoparticles depend on how rapidly the orientations of nanoparticle dipoles can be switched in an alternating magnetic field [1–5]. For therapeutic hyperthermia and magnetic particle imaging, the frequency range is typically 0.1–1 MHz, and the particles are often immobilized, so that dipolar re-orientation must occur inside the particles. As a result, even if the physical size of the particles is well controlled, it is their internal magnetic structure that is the most important. One of the ways to study the magnetic dipole moment of nanoparticles is by measuring the magnetization curve while the nanoparticles are in a dilute colloidal dispersion in a liquid. Thanks to the orientational freedom of the nanocrystals themselves in the liquid, the field-dependent magnetization can be described by the Langevin equation: $M(\alpha) = \coth(\alpha) - 1/\alpha$, with $\alpha = \mu_0 m H / (k_B T)$, $\mu_0 = 4\pi \times 10^{-7} \text{ T A}^{-1} \text{ m}$, m is the dipole moment, H is the external field in A/m, and $k_B T$ is the thermal energy. This assumes that the colloidal dispersion is sufficiently dilute for the particles to respond individually and that the equilibrium curve is without hysteresis. The situation would be different if the particles

were immobilized. Then the orientations of the easy axes are fixed, and different behaviors are obtained depending on the magnetic anisotropy of the particles and on the orientations of the easy axes, for instance random or aligned with the external field [1]. This is crucial for said high-frequency applications, but here we focus on the magnetic characterization of dilute colloidal dispersions, where magnetic anisotropy is less of an issue.

In the absence of more information, it is usually assumed that the distribution of magnetic dipole moments in a sample with nanoparticles consists of a single log-normal distribution: $P(m) = [(2\pi)^{1/2} m \sigma]^{-1} \exp[-(\ln m - \ln m^*)^2 / (2\sigma^2)]$, where σ and m^* describe the width and the center of the distribution, respectively. Such a distribution shape is a plausible assumption, but it has not always been confirmed in systems whose magnetic distribution was studied in more detail. A notable case is that of Resovist, the iron oxide particles suitable for biomedical imaging, particles whose magnetic distribution was found to be bimodal [6,7]. Moreover, we found that iron oxide nanoparticles with a low polydispersity of the physical size can nevertheless have a very high magnetic polydispersity [8]. There are several reports of similar iron oxide nanoparticles, size monodisperse, larger than 12 nm, prepared by thermal decomposition of precursors like iron oleate, which were found to have a complicated crystalline and magnetic internal structure [9–12]. Typically, a well crystallized

* Corresponding author.

E-mail address: B.H.Erne@uu.nl (B.H. Ern  ).

magnetic core is surrounded by more defective, more highly oxidized phase, resulting in a lower than expected saturation magnetization. How well magnetic nanoparticles are crystallized and how well defined are their magnetic properties depend on the chemical synthesis procedure, as we discussed before [8]. Here, we focus on the question how to determine whether size-monodal particles are magnetically monomodal or not.

In order to extract magnetic dipole moment distributions from the magnetization curves of dilute ferrofluids, we recently implemented the non-regularized inversion method MINORIM [13]. We made our program available for different platforms via the web [14]. Our numerical approach is inspired from the model-independent analysis of colloidal size distributions from light scattering, as explained in greater detail in Ref. [13]. First, diamagnetic and possibly other linear contributions to the magnetization curve are removed by fitting the high-field part of the curve, which depends only on the average dipole moment, not its precise distribution [15]. The high-field regime starts at a user-selected value H^* . Second, the corrected curve is fitted in terms of N discrete values of the effective magnetic dipole moment m , ranging geometrically from a low to a high cutoff value. The smoothness of the calculated distribution is controlled via a number S of subsets, whose effect is to bring down the maximum number of subpopulations that can be resolved. The low cutoff value of m is given by $3k_B T / (\mu_0 H^*)$, and the high cutoff value is on the order of $k_B T / (\mu_0 \Delta H)$, with ΔH the experimental step size in the applied magnetic field near $H=0$.

In previous tests of our fitting approach, we were able to detect simultaneously the presence of nanoparticles of different sizes and to confirm the known ratio of their quantities [13]. Here, we use our inversion method to re-examine the magnetic polydispersity of different types of magnetic nanoparticles in the 5–20 nm range, particles that we earlier analyzed in terms of a single log-normal distribution of the magnetic dipole moment [8].

2. Methods

The chemical preparation and characterization of the studied magnetic nanoparticles were reported before in detail [8]. In summary, all the particles were iron oxide, capped with oleic acid, and ultimately transferred to the apolar liquid decalin. The “precipitates” were prepared by aqueous precipitation of iron salts [16]. The “spheres” were obtained by thermal decomposition of iron oleate in trioctylamine [17]. The “facets” and the “twins” were made by stepwise epitaxial growth from iron acetylacetonate precursor in diphenyl ether [18].

Transmission electron microscopy (TEM) was performed with a Tecnai 12 microscope operating at 120 kV. X-ray powder diffraction (XRD) was done with a Bruker ACS D8 Advance diffractometer. Magnetization curves were measured with a Princeton Micromag 2900 alternating gradient magnetometer (AGM) [19]. Except when indicated otherwise, the samples were dilute colloidal dispersions in decalin (volume fraction < 1%). Magnetic dipole moment distributions were obtained from the magnetization curves by fitting using the inversion method MINORIM [13,14].

3. Results and discussion

Four types of iron oxide nanoparticles will each be examined in the same way. The fitted dipole moments will be presented as an effective magnetic diameter d_{eff} , calculated on the basis of a volume magnetization of 480 kA/m for pure magnetite. The magnetic distributions are magnetization-weighted, for comparison with volume-weighted data obtained by TEM and XRD. For each system, we first examine the effect of the high-field cutoff H^* and of the fitting parameters N and S , before giving a physical discussion of the results.

Iron oxide nanoparticles prepared by aqueous precipitation are analyzed in Fig. 1: the “precipitates”. Here and with the other examined types of particles, the calculated distributions no longer depend on H^* beyond the effective size that corresponds to the

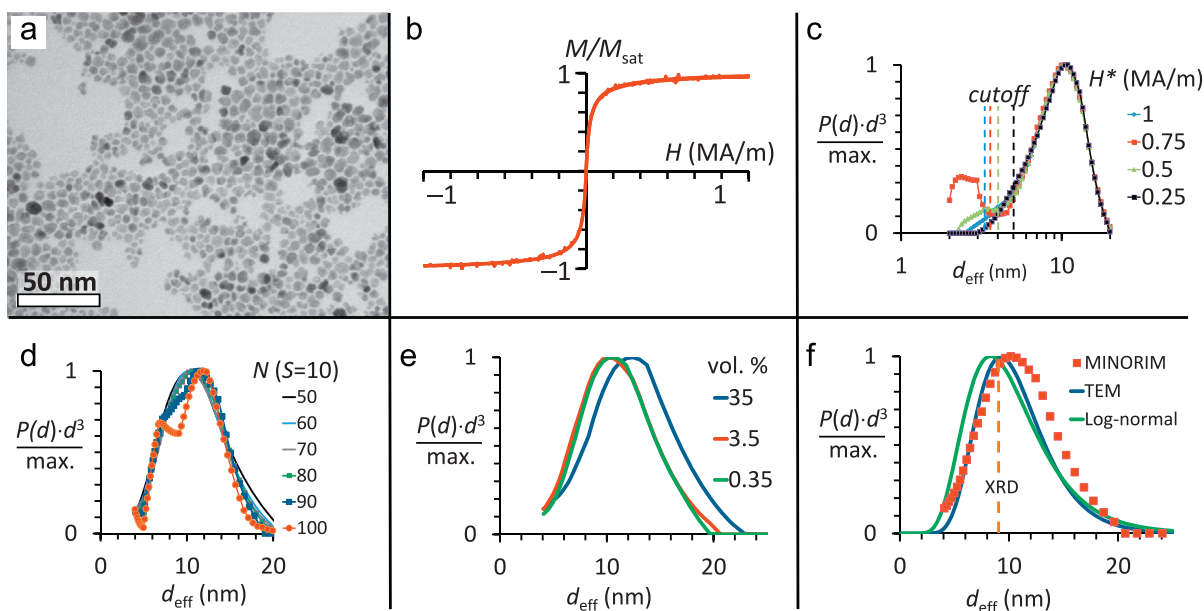


Fig. 1. Iron oxide nanoparticles prepared by wet precipitation: the “precipitates” [8]. (a) TEM micrograph, (b) magnetization curve of a liquid dispersion, and (c)–(f) analyses in terms of an effective magnetic diameter using the MINORIM inversion method [13,14]: (c) effect of the high field cutoff H^* , (d) effect of the bin sampling parameter N for $S=10$ ($H^*=0.5$ MA/m), (e) magnetic distributions obtained at three volume fractions (including 2 nm oleic acid shell; the iron oxide volume fractions are lower by a factor of 4), and (f) comparison with TEM, XRD, and a monomodal log-normal magnetic distribution [8]. The volume fraction in (b)–(d) is 3.5%, and (e) and (f) are calculated with $H^*=0.5$ MA/m, $N=60$, and $S=10$.

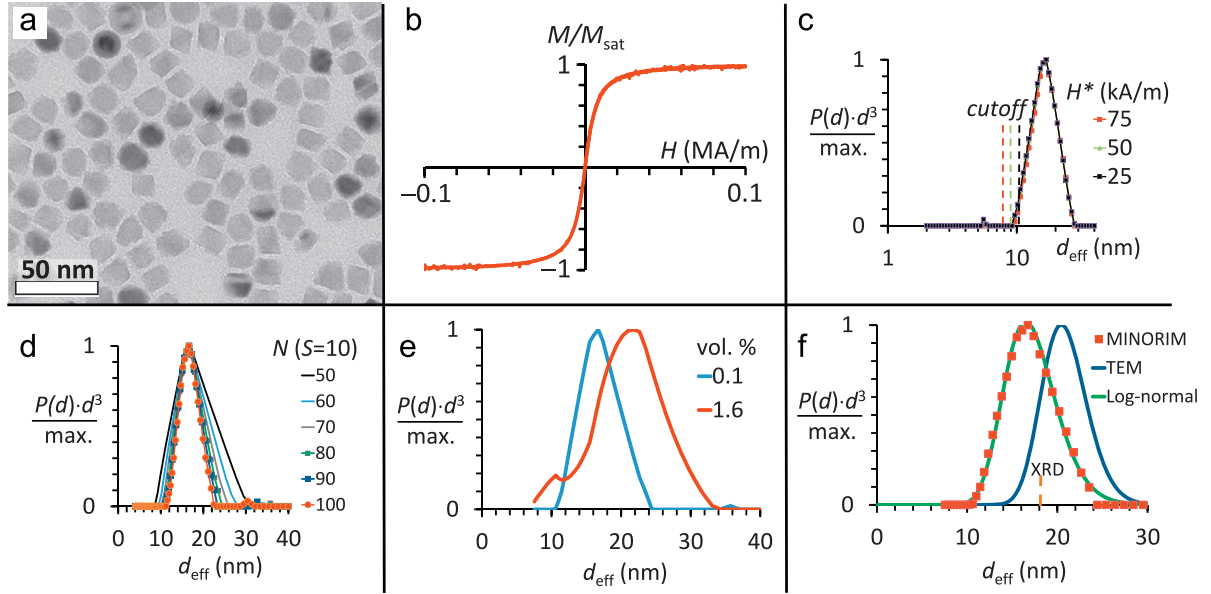


Fig. 2. Magnetite nanoparticles prepared by multistep epitaxial growth: the “facets” [8]. The subfigures are as in Fig. 1. In (c), $N=60$ and $S=10$, and in (b)–(d), and (f), the results are for a concentration of 0.1 vol% (including a 2 nm shell of oleic acid). In (e) and (f) $H^*=75$ kA/m, $N=80$, and $S=10$.

cutoff field H^* (Fig. 1c). This confirms that our mathematical approach to subtract the diamagnetic component of the magnetization curves is correct [15]. For fit parameter $S=10$ and increasing value of N , the distribution has a constant shape until $N=90$, when the monomodal distribution starts to split up, which does not appear to be physical (Fig. 1d). The ratio N/S is what determines the resolution, so that the combination of $N=50$ and $S=10$ gives the same distribution as $N=100$ and $S=20$ or as $N=200$ and $S=40$ (not shown). At high concentration of the ferrofluid, the apparent dipole moment is increased (Fig. 1e) because of dipolar interactions [20]. The shape of the distribution is log-normal, as expected from electron microscopy [21]. MINORIM finds slightly larger effective sizes than what we previously found by TEM and monomodal fitting of magnetization curves,

which were measured on a different batch of particles than those that are presented here as a function of concentration (Fig. 1e).

Fig. 2 presents the results for magnetite nanoparticles prepared by multistep epitaxial growth: the “facets”. In Fig. 2d, the effect of increasing N/S is to sharpen the distribution, in line with the relatively low polydispersity of the particles and the increasing resolution of the fits with increasing values of N/S . The concentration dependence of the effective magnetic size (Fig. 2e) is now due to dipolar chains, as we demonstrated previously using cryogenic electron microscopy [19]. There is an equilibrium distribution of dipolar chains [22,23], so that not only the average but also the width of the magnetic size distribution increases with concentration. At high dilution, the MINORIM inversion method reproduces precisely the monomodal log-normal distribution found previously (Fig. 2f) [8].

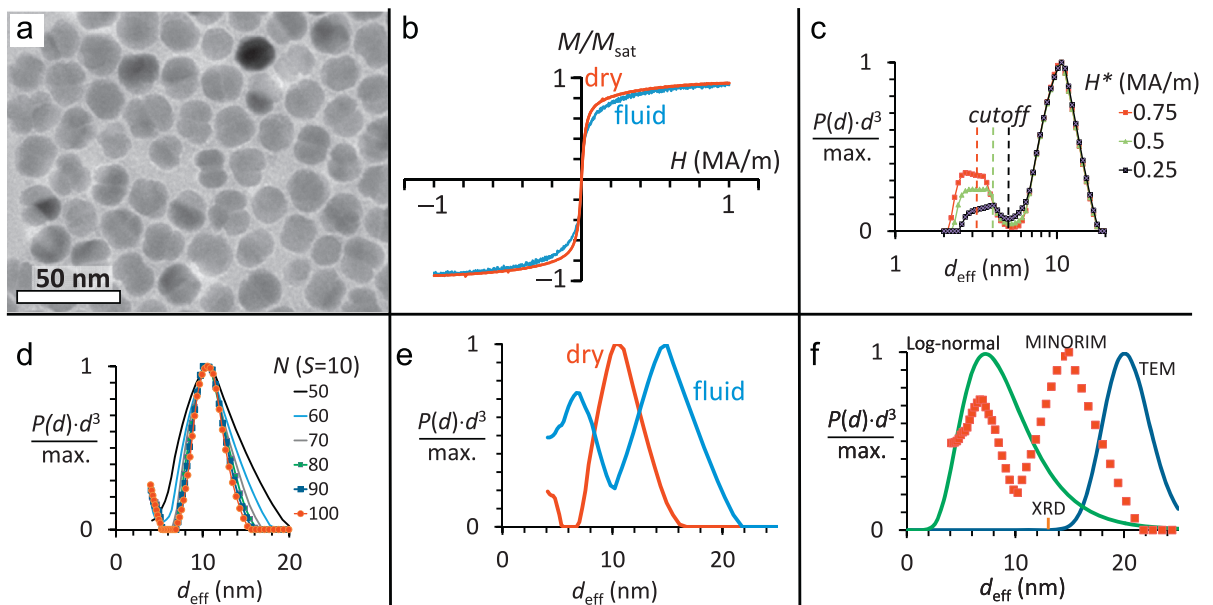


Fig. 3. Magnetite nanoparticles with twinning defects prepared by multistep epitaxial growth: the “twins” [8]. The subfigures are as in Fig. 1. In (b), (e), and (f), the concentration of particles in the fluid was 4 vol% (including oleic acid shell). In (c) ($N=60$ and $S=10$) and in (d) ($H^*=0.5$ MA/m), the results are for the dry particles. In (e) and (f), $H^*=0.5$ MA/m, $N=80$, and $S=10$.

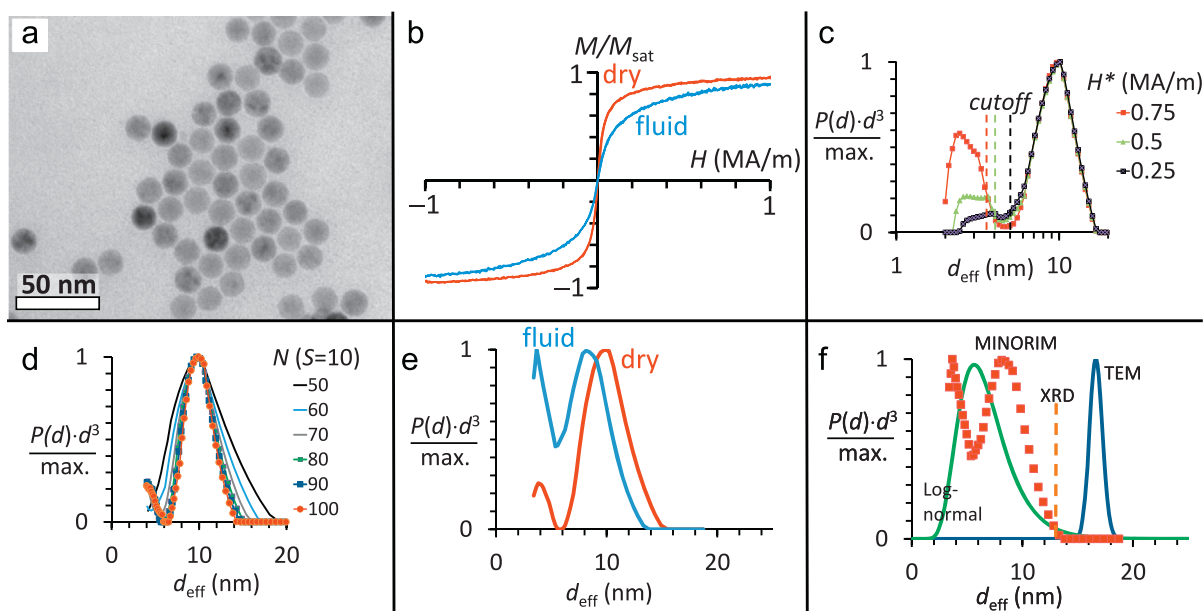


Fig. 4. Iron oxide spheres prepared by thermal decomposition of iron oleate; the “spheres” [8]. The subfigures are as in Fig. 1. In (c) ($N=60$, $S=10$) and in (d) ($H^*=0.5$ MA/m), the results are for the dry particles. In (e) and (f), $H^*=0.5$ MA/m, $N=80$, and $S=10$.

Whereas the “precipitates” and the “facets” are well crystallized, we now consider iron oxide particles that are defective. The “twins” have twinning defects (Fig. 3a), although the crystalline domains are well crystallized and consist of pure magnetite. These particles were an unsuccessful attempt to reproduce the “facet” particles by following the same chemical recipe. The magnetization curve is clearly different when the particles are dry or in liquid dispersion (Fig. 3b). Multimodal fitting reveals that the particles are magnetically bidisperse (Fig. 3e). We propose the following qualitative explanation: in an external field, the particles first tend to orient themselves in the liquid in a way that the main two crystalline domains—which are more or less parallel to each other—become magnetically aligned, and then the remaining smaller domains are aligned at higher fields. The particles appear to have effectively a higher magnetic dipole moment when dispersed in liquid than when dry. In other words, a stronger field is required to align the particles when they are immobile than when they are dispersed in a liquid. Our explanation is that when the particles are dry, the magnetic dipoles must now be re-oriented inside the particles, which is impeded by magnetic anisotropy, and since the particles touch each other, magnetic relaxation is also hampered by interparticle dipolar interactions.

The monodisperse “spheres” (Fig. 4), prepared by thermal decomposition of iron oleate, exhibit magnetic bidispersity much like the “twins”. However, the interpretation is complicated by the inhomogeneous composition of the particles. They are thought to consist of a relatively well crystallized core of Fe_3O_4 and a more oxidized, less magnetic shell phase [9,12]. We propose that the well crystallized core determines most of the net dipole moment of the particles, given by the peak at 8 nm (Fig. 4e and f), and that the peak at lower effective size is due to the shell phase. Compared to the “twins”, there is less difference between the calculated distributions when the particles are dry and when they are dispersed in a liquid. This is probably because of the lower magnetic anisotropy of the much less magnetic “spheres”. Finally, since the distribution is magnetization-weighted and the shell phase is expected to have a lower volume magnetization than the magnetite core, the distribution suggests that the volume of shell phase much exceeds that of the core. This is in line with the

effective diameter of the core (8 nm) being much smaller than the physical size (17 nm).

The possibility of having nanoparticles that are size monodisperse and magnetically bidisperse raises interesting questions about their interactions in liquid dispersions. How does their behavior compare to that of a mixture of large and small magnetically monodisperse particles, such as that studied as a model system for polydisperse ferrofluids [24–27]? We can only speculate. Two limiting cases are that (1) each particle is exactly the same, with one large magnetic domain and a less magnetic peripheral volume and (2) the particles are different from one particle to the other. In the first scenario, the structural behavior is likely to be comparable to that of monodisperse particles, although the dipole moment would depend on the external field. In the second scenario, the behavior would indeed be closer to that of a size-polydisperse system, although the particle-particle interactions would differ from those of dipolar hard spheres, due to the more complicated internal magnetic structure of the particles.

4. Conclusions

When magnetic iron oxide nanoparticles in the 5–20 nm range are well crystallized, like our “precipitates” and “facets”, the magnetic size distribution corresponds well to the distribution of the physical size. Analysis of the magnetization curve of the particles in dilute liquid dispersion diminishes effects of interparticle interactions and magnetic anisotropy of the particles. When the particles are less well crystallized, the distribution of the effective magnetic size may no longer be monomodal. With the particles dispersed in a liquid, the magnetization curve informs on the net dipole moment of the particles and on the presence of smaller magnetic domains or less magnetic phases, as demonstrated here by the “twins” and the “spheres”. Interpretation of the effective magnetic size distribution becomes relatively difficult, especially when the crystalline phase and volume magnetization of the particles are not homogeneous. Nevertheless, we conclude that the MINORIM inversion method is able to reveal when the magnetic distribution is not monomodal. This is relevant

information that would have been overlooked upon monomodal log-normal fitting.

Acknowledgements

We thank Stephan Zevenhuizen for help with the software, Bob Luigjes for electron micrographs, Rick de Groot and Suzanne Woudenberg for magnetization curves, and Aldo Brinkman, Albert Philipse, Jan Groenewold, and Quentin Harmer for helpful discussions. This work is part of the research program of the Foundation for Fundamental Research on Matter (FOM), which is part of the Netherlands Organisation for Scientific Research (NWO).

References

- [1] J. Carrey, B. Mehdaoui, M. Respaud, Simple models for dynamic hysteresis loop calculations of magnetic single-domain nanoparticles: application to magnetic hyperthermia optimization, *J. Appl. Phys.* 109 (2011) 083921.
- [2] Yu.L. Raikher, V.I. Stepanov, Physical aspects of magnetic hyperthermia: low-frequency ac field absorption in a magnetic colloid, *J. Magn. Magn. Mater.* 368 (2014) 421–427.
- [3] S. Dutz, R. Hergt, Magnetic nanoparticle heating and heat transfer on a microscale: Basic principles, realities and physical limitations of hyperthermia for tumour therapy, *J. Hyperth.* 29 (2013) 790–800.
- [4] K.M. Krishnan, Biomedical nanomagnetism: a spin through possibilities in imaging, diagnostics, and therapy, *IEEE Trans. Magn.* 46 (2010) 2523–2558.
- [5] Q.A. Pankhurst, J. Connolly, S.K. Jones, J. Dobson, Applications of magnetic nanoparticles in biomedicine, *J. Phys. D: Appl. Phys.* 36 (2003) R167–R181.
- [6] A.F. Thünemann, S. Rolf, S. Weidner, In situ analysis of a bimodal size distribution of superparamagnetic nanoparticles, *Anal. Chem.* 81 (2009) 296–301.
- [7] D. Eberbeck, F. Wiekhorst, S. Wagner, N. Löwa, L. Trahms, How the size distribution of magnetic nanoparticles determines their magnetic particle imaging performance, *Appl. Phys. Lett.* 98 (2011) 182502.
- [8] B. Luigjes, S.M.C. Woudenberg, R. de Groot, J.D. Meeldijk, H.M. Torres Galvis, K. P. de Jong, A.P. Philipse, B.H. Ern , Diverging geometric and magnetic size distributions of iron oxide nanocrystals, *J. Phys. Chem. C* 115 (2011) 14598–14605.
- [9] A. Lak, M. Kraken, F. Ludwig, A. Kornowski, D. Eberbeck, S. Sievers, F.J. Litterst, H. Weller, M. Schillinga, Size dependent structural and magnetic properties of FeO–Fe₃O₄ nanoparticles, *Nanoscale* 5 (2013) 12286–12295.
- [10] M. Levy, A. Quarta, A. Espinosa, A. Figuerola, C. Wilhelm, M. Garc a-Hern andez, A. Genovese, A. Falqui, D. Alloyeau, R. Buonsanti, P.D. Cozzoli, M.A. Garc a, F. Gazeau, T. Pellegrino, Correlating magneto-structural properties to hyperthermia performance of highly monodisperse iron oxide nanoparticles prepared by a seeded-growth method, *Chem. Mater.* 23 (2011) 4170–4180.
- [11] B.P. Pichon, O. Gerber, C. Lefevre, I. Florea, S. Fleutot, W. Baaziz, M. Pauly, M. Ohlmann, C. Ulhaq, O. Ersen, V. Pierron-Bohnes, P. Panissod, M. Drillon, S. Begin-Colin, Microstructural and magnetic investigations of w stite–spinel core–shell cubic-shaped nanoparticles, *Chem. Mater.* 23 (2011) 2886–2900.
- [12] W. Baaziz, B.P. Pichon, S. Fleutot, Y. Liu, C. Lefevre, J.-M. Greneche, M. Toumi, T. Mhiri, S. Begin-Colin, Magnetic iron oxide nanoparticles: reproducible tuning of the size and nanosized-dependent composition, defects, and spin canting, *J. Phys. Chem. C* 118 (2014) 3795–3810.
- [13] J. van Rijssel, B.W.M. Kuipers, B.H. Ern , Non-regularized inversion method from light scattering applied to ferrofluid magnetization curves for magnetic size distribution analysis, *J. Magn. Magn. Mater.* 353 (2014) 110–115.
- [14] (<http://hdl.handle.net/10411/10164>).
- [15] See the supporting information of Ref. [13].
- [16] D. Bica, Preparation of magnetic fluids for various applications, *Rom. Rep. Phys.* 47 (1995) 265–272.
- [17] J. Park, K. An, Y. Hwang, J.-G. Park, H.-J. Noh, J.-Y. Kim, J.-H. Park, N.-M. Hwang, T. Hyeon, Ultra-large-scale syntheses of monodisperse nanocrystals, *Nat. Mater.* 3 (2004) 891–895.
- [18] M. Klokkenburg, C. Vonk, E.M. Claesson, J.D. Meeldijk, B.H. Ern , A.P. Philipse, Direct imaging of zero-field dipolar structures in colloidal dispersions of synthetic magnetite, *J. Am. Chem. Soc.* 126 (2004) 16706.
- [19] M. Klokkenburg, B.H. Ern , V. Mendelev, A.O. Ivanov, Magnetization behavior of ferrofluids with cryogenically imaged dipolar chains, *J. Phys.: Condens. Matter* 20 (2008) 204113.
- [20] A.O. Ivanov, O.B. Kuznetsova, Magnetogranulometric analysis of ferrocolloids: second-order modified mean field theory, *Colloid J.* 68 (2006) 430–440.
- [21] B.H. Ern , E. van den Pol, G.J. Vroege, H.H. Wensink, Size fractionation in a phase-separated colloidal fluid, *Langmuir* 21 (2005) 1802–1805.
- [22] M. Klokkenburg, R.P.A. Dullens, W.K. Kegel, B.H. Ern , A.P. Philipse, Quantitative real-space analysis of self-assembled structures of magnetic dipolar colloids, *Phys. Rev. Lett.* 96 (2006) 037203.
- [23] M. Klokkenburg, B.H. Ern , J.D. Meeldijk, A. Wiedenmann, A.V. Petukhov, R.P. A. Dullens, A.P. Philipse, In situ imaging of field-induced hexagonal columns in magnetite ferrofluids, *Phys. Rev. Lett.* 97 (2006) 185702.
- [24] T. Kruse, A. Spanoudaki, R. Pelster, Monte Carlo simulations of polydisperse ferrofluids: cluster formation and field-dependent microstructure, *Phys. Rev. B* 68 (2003) 054208.
- [25] A.O. Ivanov, S. Kantorovich, Chain aggregate structure and magnetic birefringence in polydisperse ferrofluids, *Phys. Rev. E* 70 (2004) 021401.
- [26] C. Holm, A. Ivanov, S. Kantorovich, E. Pyanzina, E. Reznikov, Equilibrium properties of a bidisperse ferrofluid with chain aggregates: theory and computer simulations, *J. Phys.: Condens. Matter* 18 (2006) S2737–S2756.
- [27] E. Novak, E. Minina, E. Pyanzina, S. Kantorovich, A. Ivanov, Structure factor of model bidisperse ferrofluids with relatively weak interparticle interactions, *J. Chem. Phys.* 139 (2013) 224905.